AD

TECHNICAL REPORT ARCCB-TR-01012

ABLATIVE EROSION MODEL FOR
THE M256/M829E3 GUN SYSTEM

SAMUEL SOPOK
MARK FLESZAR

JUNE 2001

US ARMY ARMAMENT RESEARCH,
DEVELOPMENT AND ENGINEERING CENTER
CLOSE COMBAT ARMAMENTS CENTER
BENÉT LABORATORIES
WATERVLIET, N.Y. 12189-4050

20010712 075

DISCLAIMER

The findings in this report are not to be construed as an official Department of the Army position unless so designated by other authorized documents.

The use of trade name(s) and/or manufacturer(s) does not constitute an official endorsement or approval.

DESTRUCTION NOTICE

For classified documents, follow the procedures in DoD 5200.22-M, Industrial Security Manual, Section II-19, or DoD 5200.1-R, Information Security Program Regulation, Chapter IX.

For unclassified, limited documents, destroy by any method that will prevent disclosure of contents or reconstruction of the document.

For unclassified, unlimited documents, destroy when the report is no longer needed. Do not return it to the originator.

REPORT DOCUMENTATION PAGE

1. AGENCY USE ONLY *(Leave blank)*	2. REPORT DATE	3. REPORT TYPE AND DATES COVERED
	June 2001	Final

4. TITLE AND SUBTITLE

ABLATIVE EROSION MODEL FOR
THE M256/M829E3 GUN SYSTEM

5. FUNDING NUMBERS

PRON No. 4A0D0FYK1ABJ

6. AUTHOR(S)

Samuel Sopok and Mark Fleszar

7. PERFORMING ORGANIZATION NAME(S) AND ADDRESS(ES)

U.S. Army ARDEC
Benet Laboratories, AMSTA-AR-CCB-O
Watervliet, NY 12189-4050

8. PERFORMING ORGANIZATION REPORT NUMBER

ARCCB-TR-01012

9. SPONSORING / MONITORING AGENCY NAME(S) AND ADDRESS(ES)

U.S. Army ARDEC
Close Combat Armaments Center
Picatinny Arsenal, NJ 07806-5000

10. SPONSORING / MONITORING AGENCY REPORT NUMBER

11. SUPPLEMENTARY NOTES

Presented at the 37th JANNAF Combustion Meeting, Monterey, CA, 13-17 November 2000.
Published in proceedings of the meeting.

12a. DISTRIBUTION / AVAILABILITY STATEMENT

Approved for public release; distribution unlimited.

12b. DISTRIBUTION CODE

13. ABSTRACT *(Maximum 200 words)*

A combination of bore-protecting ablative and bore-coating technologies is necessary to reduce erosion for current and future high-performance gun systems. Our cannon coating erosion model developed in 1996 is fully capable of incorporating the added complexity of bore-protecting ablatives. Both nonablative and ablative results from this model have been published for a number of important Army and Navy gun systems with bore coatings. This erosion model is guided and calibrated and correlates very well with substantial gun system firing data and subsequent laboratory analysis of fired specimens. Additionally, the model uses measured ablative flow and thermal decomposition data to determine the ablative mechanisms and guide/calibrate ablative modeling. The purpose of this report is to show how our ablative model incorporates into our overall cannon coating erosion code by using the experimental ablative M256/M829E3 gun system as an illustrative example. Although we do not have authority to release the composition and processing of this proprietary ablative paste, we do have authority to release its general thermal decomposition, flow characteristics, and ablative mechanism data. These decomposition, flow, and ablative mechanism data are used by the thermochemical, boundary layer, and thermal and erosion modeling codes to include the effect of the ablative paste and its associated thermal decomposition products. Experimental ablative M829E3 rounds-to-erosion condemnation at the peak eroded 1.6-meter from the rear face of the tube position determines this gun system's predicted erosion life. At that position, the respective 49°C, 21°C, and -32°C round-conditioning temperature cases achieve predicted erosion condemnation at approximately 240, 390, and 350 rounds.

14. SUBJECT TERMS

Ablative Erosion Modeling, M256 Tank Guns, M829E3 Tank Rounds

15. NUMBER OF PAGES

20

16. PRICE CODE

17. SECURITY CLASSIFICATION OF REPORT	18. SECURITY CLASSIFICATION OF THIS PAGE	19. SECURITY CLASSIFICATION OF ABSTRACT	20. LIMITATION OF ABSTRACT
UNCLASSIFIED	UNCLASSIFIED	UNCLASSIFIED	UL

TABLE OF CONTENTS

LIST OF ILLUSTRATIONS

INTRODUCTION

Our initial rocket-derived model that was introduced in 1995 was quite successful for predicting erosion on uncoated and nitrided steel cannon bores (ref 1). Our cannon coating erosion model developed in 1996 is fully capable of incorporating the added complexity of bore-protecting ablatives (ref 2). Both nonablative and ablative results from this model have been published for a number of important Army and Navy gun systems with bore coatings. This cannon erosion model consists of a number of linked thermochemistry, interior ballistic, boundary layer, thermal, erosion, and bore-coating codes. These codes are used to predict wall temperature profiles and erosion profiles in bore-coated cannons as a function of position, time, and round history.

Pressure gauge, radar, thermocouple, and kinetic rate data are used to calibrate these codes. The codes receive important inputs from nondestructive and laboratory microscopic materials/chemical analyses of fired specimens. The analyses focus on substrate exposure, coating loss, cracks, pits, interfaces, voids, and surfaces, including their crack/pit frequency, crack/pit width, coating platelet width, wall layers, residues, reactions, diffused species, and phase changes all as a function of position, time, and round history.

Our original experimental M829E3 modeling effort (ref 3) included 19 pounds of RPD-380 propellant and a classified projectile F-slug weight. The RPD-380 propellant fracturing was not allowed at -32°C despite its glass transition at -29°C, both with/without one pound of ablative paste on a moving projectile base donut. Ablative paste products were not allowed on the bore wall if present.

Our next experimental M829E3 modeling effort (ref 2) included 18 pounds of RPD-380 propellant and a 0.3-pound lighter classified projectile F-slug weight than the original effort. The RPD-380 propellant fracturing was allowed at -32°C due to its glass transition at -29°C, with no ablative paste.

This experimental M829E3 modeling effort also includes 18 pounds of RPD-380 propellant and a 0.3-pound lighter classified projectile F-slug weight than the original effort. Then RPD-380 propellant fracturing was allowed at -32°C due to its glass transition at -29°C, with 0.5-pound of ablative paste on the combustible case shoulder. Ablative paste products were allowed on the bore wall.

COMPUTATIONAL AND EXPERIMENTAL METHODS

Our Cannon Coating Erosion Code consists of a number of interactively linked codes and is used to predict wall temperature profiles and thermal-chemical-mechanical erosion profiles in cannons (refs 1-3). This overall erosion code includes the following:

- CCET thermochemistry cannon code (refs 1-4)
- XNOVAKTC interior ballistics code (refs 1-3,5)
- MABL boundary layer cannon code (refs 1-3,6),
- MACE thermal and erosion cannon code (refs 1-3,7)

These erosion predictions are guided and calibrated by substantial gun system firing data and fired specimen analyses. The M829E3 modeling effort uses 18 pounds of RPD-380 propellant and a 0.3-pound lighter classified projectile F-slug weight than a previous effort (ref 2). The RPD-380 propellant fracturing was allowed at -32°C due to its glass transition at -29°C, with 0.5 pound of ablative paste on the combustible case shoulder. Ablative paste products were allowed on the bore wall.

RESULTS AND DISCUSSION

The experimental ablative M829E3 kinetic energy tank round fired from the M256 cannon is used to show how the ablative cannon erosion model is incorporated into the overall cannon erosion code. The CCET thermochemistry cannon code is the first step in the overall analysis. It uses chemical and material inputs to calculate gas/gas thermochemistry data for the interior ballistics, boundary layer, and thermal and erosion codes. The example M829E3/RPD-380 propellant consists of approximately 59% nitrocellulose, 25% nitroglycerine, 15% diethylene glycol dinitrate, and 1% other minor species. Its igniter consists of 25 grams black powder and 25 grams CBI. Measured thermochemical data are used to calibrate the calculation for gas/gas products.

The XNOVAKTC interior ballistics code uses thermochemistry code output and gun system defining inputs to calculate the time-dependent core flow data for the boundary layer code. This gun system includes the 17.3-foot 120-mm M256 cannon, its experimental 18-pound RPD380 propellant, its experimental 0.5-pound proprietary ablative, and classified projectile details. Measured pressure gauge and muzzle velocity data are used to calibrate this time-dependent core flow calculation.

Figures 1 and 2 show XNOVAKTC interior ballistics results for the experimental ablative M829E3 round. These figures respectively give maximum values of gas pressure (P_g) and gas temperature (T_g) as a function of selected axial positions at selected round-conditioning temperatures. Maximum values were used instead of time-dependent data to compare the three round-conditioning temperatures. Both the P_g and T_g decrease with increasing axial position. Gas velocity is omitted due to its classified nature. Selected axial positions included 0.6, 1.6, 2.2, 3.3, and 5.1 meters from the rear face of the tube (RFT), while the selected round-conditioning included the hot (49°C), ambient (21°C), and cold (-31°C) temperatures. These five selected axial positions and three selected round-conditioning temperatures were used exclusively throughout the rest this study.

In Figures 1 and 2, the significance of the 0.6-meter position is that it is slightly past the origin of the bore, and it is the mean peak eroded position when both M829E3 and HEAT-type rounds are mixed. The significance of the 1.6-meter position is that it is the mean peak eroded

position when M829E3 rounds are fired without HEAT-type rounds. The significance of the 2.2-meter position is that it is the mean peak eroded position when M829A2 rounds are fired in the M256 cannon without HEAT-type rounds. The significance of the 3.3-meter position is that it is near the bore evacuator holes. The significance of the 5.1-meter position is that it is near the muzzle. Statistical distributions exist around these various mean eroded positions.

The MABL boundary layer cannon code uses thermochemistry and interior ballistics code outputs to calculate boundary layer characteristics for the thermal and erosion code. Figures 3 and 4 show the MABL boundary layer results for the experimental ablative M829E3 round. These figures respectively give maximum values of recovery enthalpy (H_r) and cold wall heat flux (Q_{cw}) as a function of selected axial positions at selected round-conditioning temperatures. Maximum values were again used instead of time-dependent data to compare the three round-conditioning temperatures. In these figures, both H_r and Q_{cw} increase with increasing axial position to a 1.6-meter from RFT peak and decrease thereafter to the muzzle. The 0.6-meter from RFT peak heat transfer position calculated by the interior ballistics analysis is shifted to a 1.6-meter from RFT peak position due to the added boundary layer analysis. This is due to inclusion of the 1600°K combustible case gas cooling effects and turbulent gas mixing/heating effects.

The CCET thermochemistry cannon code uses initial chemical and materials input to calculate gas/wall thermochemistry data for the thermal and erosion code. Measured thermochemical data are used to calibrate the calculation for gas/wall products and gas/wall reaction rates. Figure 5 shows the CCET thermochemical results for the experimental ablative M829E3 round. Simplified mean values are given for the reacting gas/wall enthalpy (H_{gw}) and thermochemical ablation potential (B_a) as a function of wall temperatures (T_{wall}) for the high contraction (HC) chromium plate/gun steel substrate wall materials.

The MACE thermal and erosion cannon code uses thermochemistry code output, boundary layer code output, material properties input, and firing history and scenario input to calculate wall temperature profiles and thermal-chemical-mechanical wall erosion profiles. These predicted results are given as a function of axial position, radial position, time, and firing history and scenario.

The following data types are used to calibrate the wall thermal and erosion calculation:

- Measured gas/wall kinetic rate function input data
- Measured thermocouple input data
- Measured destructive/nondestructive microscopic coating and steel loss (void) input data (cracks, pits, interfaces, surfaces)
- Measured destructive reaction/diffusion/phase change degradation layer input data (cracks, pits, interfaces, surfaces)

For this ablative round, ablative paste decomposition and viscosity data are measured as a function of temperature to calibrate the wall thermal and erosion calculation for ablative effects.

3

Measured gas/wall kinetic rate function data are used to calibrate the thermochemical calculation and transform this chemical equilibrium calculation into a partial chemical kinetic calculation. Chemical analysis of crack and pit wall layers, interface wall layers, bore surface layers, subsurface void residues, and surface residues further guide gas/wall kinetics calibration. Thermocouple data are used to calibrate the wall thermal profile calculation.

Figure 6 shows typical gun steel substrate exposure for cannons with a mixture of experimental M829E3 rounds and other kinetic energy rounds. These data are from a small sampling of HC chromium plated M256 cannons that typify cracking, pitting, and chromium plate loss. This small sampling of cannons was condemned on erosion and had numerous condemning scoring holes centered at the 1.6-meter from RFT position. The substrate exposure is a function of the selected axial positions at 1% (nondestructively measured at post-proofing), 50% (exponentially estimated), 80% (exponentially estimated), and 100% (nondestructively and destructively measured at erosion condemnation) of equivalent ambient-conditioned M829E3 erosion life based on previous work (ref 2).

The nondestructive substrate exposure measurements are taken by a magnifying borescope with a calibrated scale, while the corresponding destructive measurements are taken by metallographic and scanning electron microscopic techniques. These nondestructive measurements are based on the verified assumption that substrate exposure is approximately equal at the surface and interface. Bore position-dependent and equivalent erosion life-dependent substrate exposure measurements include axial and circumferential crack/pit frequency, axial and circumferential crack/pit width, and axial and circumferential platelet width. These measured data are used as a substitute for a thermal-mechanical crack and pit model that is yet to be developed. The measured substrate exposure pattern correlates with the boundary layer heat transfer pattern where both increase with increasing axial position to a 1.6-meter from RFT peak and decrease thereafter to the muzzle.

Micrographic examples of destructive substrate exposure measurements were described previously (refs 2,3). These measurements were taken by metallographic and scanning electron microscopic techniques. For the M829E3 peak eroded position of 1.6 meters from RFT, the micrographs illustrate typical enabling and accelerating erosion mechanism steps. One micrograph shows a very fine HC chromium plate crack that provides a narrow combustion gas path to the gun steel producing limited interfacial gun steel degradation. Another micrograph shows a progressively widened/extended HC chromium plate crack due to chromium shrinkage that provides a wide combustion gas path to the gun steel producing substantial interfacial gun steel degradation, which leads to eventual spalling of the associated chromium platelet. Using these techniques, coupled with their associated chemical analysis techniques, the subject and similar micrographs illustrate phase change degradation (diffusion-induced carburized white layer and heat-affected zone on/into exposed gun steel, chromium recrystallization) and chemical reaction degradation (oxidation and sulfidation of exposed gun steel forming semi-metallic layers) of the gun steel substrate under the 130-µm thick chromium plate and particularly at crack and interfacial walls/wall layers.

The HC chromium plate has a passivating oxidation temperature at about 2000°K, a sulfidation temperature above 2130°K, and a melting point at about 2130°K. Gun steel has an expansive flaking iron oxidation temperature at about 1050°K, an iron sulfidation temperature at about 1270°K, an iron oxide melting point at about 1640°K, an iron sulfide melting point at about 1470°K, and a gun steel melting point at about 1720°K.

The combustion gases oxidize and corrode the interfacial gun steel through chromium cracks. These oxidized steel products require a larger volume than the uncorroded steel. This increased corrosion volume progressively forces the chromium platelet-interface apart, as the interfacial corrosion worsens. This plays a significant role in chromium platelet spalling.

Although we do not have authority to release the composition and processing of the proprietary ablative paste, we do have authority to release its general thermal decomposition, flow characteristics, and ablative mechanism. The decomposition, flow, and ablative mechanism data are used by the thermochemical, boundary layer, and thermal and erosion modeling codes to include the effect of the ablative paste and its associated thermal decomposition products.

Figure 7 presents ablative paste thermal decomposition data for the experimental M829E3 gun system. This figure plots thermal analysis weight per initial weight as a function of temperature. The ablative paste begins to generate formaldehyde, carbon monoxide, carbon dioxide, water, and hydrogen at about 420°K. The paste has a flash point of about 590°K and is about 90% decomposed to products and residue at 810°K. At about 1190°K, the ablative paste is completely decomposed to products and residue. This final residue is only about 69% of its initial ablative paste weight and consists of two ceramic oxides.

Figure 8 shows ablative paste thermal viscosity data for the experimental M829E3 gun system. The figure plots thermal analysis viscosity per initial viscosity data as a function of temperature. Due to exponentially accelerating ablative paste decomposition that initiates from the 420° to 590°K chemical decomposition onset range given in Figure 7, this increasing decomposition with temperature results in decreasing viscosity. The paste has lost about 90% of its viscosity at 810°K. At about 1190°K, the initial ablative paste has completely decomposed resulting in zero viscosity.

Figures 9 through 11 show the respective experimental ablative M829E3 MACE maximum wall temperature (T_{wall}) results for the HC chromium surface, gun steel interface, and gun steel surface minus 0.13-mm as a function of the selected axial positions at the selected round-conditioning temperatures. For these figures, maximum values were also used instead of time-dependent data to compare round-conditioning temperatures. The maximum wall temperature for the HC chromium surface is about 1590°K, which explains its inertness. The maximum wall temperature for the unexposed nonreacting gun steel interface is about 1250°K, which explains its reactivity. The maximum wall temperature for the fully exposed reacting gun steel surface (0.13-mm below bore surface due to HC chromium spalling) is about 1390°K, which explains its reactivity. For these three figures, the calculated maximum wall temperature patterns correlate with the boundary layer heat transfer pattern, where both increase with increasing axial position to a 1.6-meter from RFT peak and decrease thereafter to the muzzle.

5

Core flow gases at the combustion gas temperature collide with the bore surface and convectively transfer a portion of their energy to the wall. This fully convective bore surface heating is related to the bore surface temperature.

When a bore coating platelet spalls forming a pit that is at least 33% wider than the coating thickness depth, a portion of the core flow combustion gases collide with the exposed substrate interface and convectively transfer a portion of their energy to this interface at a rate approximately equal to that at the bore surface. The fully convective substrate interface heating is related to that exposed substrate interface temperature and approximately equal to the fully exposed substrate bore surface temperature that is actually 0.13-mm below the original bore surface due to HC chromium spalling. The wide pit-maximum convective heating of the substrate interface is designated case one. The HC chromium coating thickness is typically 0.005-inch, and the minimum required pit width for fully convective heating is about 0.0067-inch for the experimental M829E3 round.

When a bore coating platelet spalls forming a pit that is progressively narrower than case one's pit width, a progressively decreasing portion of the core flow combustion gases collide with the partially exposed substrate interface. This results in the convective transfer of a portion of the energy to this partially exposed interface at a rate that is progressively less than that of the fully exposed substrate bore surface due to the increase of energy-reducing collisions. This progressively decreasing convective substrate interface heating is related to the partially exposed substrate interface temperature, and is progressively less than the above exposed gun steel bore surface temperature. As the crack/pit width progressively narrows, the mean free path of the gas molecules decreases due to energy-reducing collisions prior to the interface that reduce the convective heat transfer rate to a value that is progressively closer to that of the unexposed conductive heat transfer rate of the interface. The transition from wide to infinitesimally small crack/pit-transition from maximum to infinitesimally small convective heating of the substrate interface is designated case two.

When a bore coating has a very fine crack forming an infinitesimally narrow pit, the core flow combustion gases never reach the substrate interface without many energy-reducing collisions that reduce the convective heat transfer rate to that of the unexposed substrate interface conductive heat transfer rate. The infinitesimally small convective substrate interface heating is related to that interface temperature and approximately equal to the fully conductive unexposed substrate interface temperature. This model includes initial high-pressure filling of cracks and pits. The infinitesimally small crack/pit with infinitesimally small convective heating of the substrate interface is designated case three. Very fine HC chromium crack widths are typically 0.00005-inch for the experimental M829E3 round.

A cubic function of the general form $y = a + bx^3$ uses the above fully convective heating case one and fully conductive heating case three extremes for calibration to predict a resultant substrate interface temperature for a given crack/pit width as follows:

$$T_{iy} = T_{iu} + [((T_s - T_{iu})/W_c^3)(W_x^3)] \tag{1}$$

6

where

- T_{iy} is the resultant calculated substrate interface temperature for a given crack/pit width.
- T_{iu} is the calculated fully conductive/unexposed substrate interface temperature of a very small crack/pit width, which is approximately equal to the fully conductive/unexposed substrate interface temperature from Figure 10.
- T_s is the calculated fully convective/exposed substrate surface temperature for crack/pit width that is at least 33% greater than the coating thickness depth, which is approximately equal to the fully exposed reacting substrate surface temperature from Figure 11 (substrate surface is 0.13-mm below the bore surface due to HC chromium spalling).
- W_c is the measured fully convective/exposed crack/pit width that is at least 33% greater than the coating thickness depth from micrographs described in Reference 2.
- W_x is a measured given crack/pit width from substrate exposure data that generated Figure 6.

The first term on the right is the y-intercept that is the substrate interface temperature due to conductive heating. The second term on the right (in brackets) is the associated temperature correction for convective heating that ranges from infinitesimally small to the difference between $T_s - T_{iu}$. The T_{iy} value changes slowly at first with increasing W_x and then more rapidly as it approaches W_c due to the cubic function. For similar cracks/pits, T_{iy} in this equation varies significantly with axial position, time, and rounds history. Exposed substrate interface temperatures are calculated for the life of each crack and pit. For a gun system that has not been built or fired, crack/pit data can possibly be approximated from a similar gun system. Using this equation, Figure 12 shows the calibrating extreme measured points and the calculated interior points for the nonablative M829E3 maximum exposed interface temperature as a function of HC chromium crack/pit width at selected axial positions and 49°C round conditioning.

An exponential fit was also used and gave very similar results compared to this cubic function. Since the meaning of the coefficients for the cubic function was easier to determine compared to that of the exponential function, we opted to use the better-understood cubic fit given in equation (1). For the cubic fit in equation (1), it is important to note that its "constant" coefficients are not really constant and vary by axial position, time, rounds history, and gun system.

Equation (1) correlates with and has been successfully applied to numerous advanced medium and large caliber gun systems over the last four years, based on measured firing-related data from their most extreme rounds. The measurements include phase change degradation data (diffusion-induced carburized white layer and heat-affected zone on/into exposed gun steel, chromium recrystallization) and chemical reaction degradation data (oxidation and sulfidation of exposed gun steel forming semi-metallic layers). The existence and depth of these measured degradations into the exposed gun steel substrate depends on and correlates with the magnitude of the related positional-dependent wall temperature profiles. These measurements were particularly focused on the exposed gun steel substrate at the crack/pit/interface walls and wall layers.

7

After the resultant substrate interface temperatures in cracks/pits are calculated for the position, time, and round-dependent crack/pit widths, the heat transfer multipliers in the MACE code are adjusted on a trial and error basis to achieve the resultant substrate interface temperatures and their corresponding substrate interface ablation rates. The adjustment of these heat transfer multipliers raises the associated T_{iu} values to the resultant T_{iy} values. Surface ablation rates are calculated directly by the MACE code and do not require a previous calculation using equation (1). In addition, as the measurable interface degradation progresses, the interface contact variable in the MACE code is adjusted as a function of axial position and rounds history. The transition from fully-conductive to fully-convective substrate interface temperature extremes is computed for the erosion life of each crack and pit based on position, time, and round-dependent substrate exposure data. Exposed substrate interface ablation rates are calculated for the life of each crack and pit.

Steel substrate degradation of interfaces, cracks, pits, and surfaces is computed by the area under a temperature-time curve above a degradation threshold such as:

- The 1000°K transformation onset of steel
- The 1050°K oxidation onset of iron by oxygen
- The 1270°K oxidation onset of iron by sulfur
- The 1420°K melting point onset of iron carbide white layer eutectic
- The 1470°K melting point onset of the iron-sulfur compound
- The 1640°K melting point onset of the iron-oxygen compound
- The 1720°K melting point onset of gun steel

Calibrated diffusion-controlled transformation codes are used to evaluate multi-component gun steel system transformations.

The exposed steel interface degradation thickness is measurable as a function of position and round history. This exposed steel interface degradation thickness under a chromium platelet is consumed in a linear strand-burning fashion by the associated T_{iy} ablation rate above the ablation threshold. When any type of degradation of the exposed gun steel interface thickness under this coating platelet merges from all adjacent cracks/pits, the coating platelet spalls and gas wash onset begins.

Heat and diffused species are transferred inward in an exponentially-decaying fashion from exposed steel substrate interface crack/pit walls surrounding an unexposed substrate interface thickness under a coating platelet. Extreme heating and diffusion of the substrate interface thickness results in transformation, interstitial occupation, and reactions that may merge leading to complete degradation of the interface thickness, subsequent mechanically-assisted bore coating platelet spalling, and substrate gas wash. This transformation of the gun steel substrate to untempered martensite merges inward from all adjacent crack/pit walls leading to complete degradation of the interface and subsequent coating platelet spalling. In a similar fashion but to a lesser extent and lesser-associated distance inward, diffusion species are transferred inward from all adjacent crack/pit walls in an exponentially-decaying fashion. These

8

diffused species result in interstitial occupation and/or reactions of the gun steel substrate, thus leading to degradation of the interface and subsequent coating platelet spalling.

Continued firing of all coated cannons results in eventual heat checking of their bore coatings. A crack or pit of any kind in the brittle M256 HC chromium coating provides a mass transport path to the gun steel. Severe (wide) or frequent bore coating heat-checking cracks/pits result in respective exponential and linear growth of erosion. Increasing either exposes the gun steel substrate interface to more hot combustion gases. Using nondestructive and laboratory microscopic analyses of fired specimens, it is important to measure how much of the steel substrate is exposed as a function of position, time, and firing history/scenario. Progressively increasing the crack or pit width for a given crack frequency and heating profile results in exponential growth of the exposed substrate interface temperature. This is due to increased convective heating of that interface from increased core flow gas collisions. Progressively increasing the crack or pit frequency (decreasing both the interface and coating platelet widths) for a given crack width and heating profile results in linear growth of the bi-directional percentage of substrate interface degradation under a bore coating platelet due to decreasing the degradation's merging distance.

Additionally, exponential growth of erosion results from progressive temperature increases above each of the mentioned gas/wall reaction thresholds due to exponential growth of combustion gas/exposed substrate interface reactions. Again, using nondestructive and laboratory microscopic materials/chemical analyses of fired specimens, it is important to measure the achievement of and level above these reaction thresholds as a function of position, time, and round history. Based on the Arrhenius equation, the reaction rate above the combustion gas/exposed interfacial substrate wall reaction threshold rises exponentially with increasing temperature. Combustion gas chemistry plays a role in increasing gas/wall reaction rates. This bore coating erosion model requires measurable gas/wall bore coating and steel substrate reactivity data as a function of pressure, temperature, and velocity. When these data are not available in the literature, they are measured in-house for each gun system material/configuration using specialized gas/wall kinetic rate/Arrhenius testers.

Figures 13 and 14 show the experimental ablative M829E3 round cumulative erosion predictions. These include the respective values of cumulative rounds to 0.13-mm erosion (gun steel gas wash onset) and 5-mm erosion (erosion condemnation) as a function of the selected axial positions at selected round-conditioning temperatures. The data in these two figures inversely correlate with the predicted M829E3 boundary layer heat transfer and substrate exposure patterns above where the erosion values decreased to a 1.6-meter from RFT minimum and increased thereafter. In Figure 13, the chromium plate loss at the muzzle is due to purely mechanical effects.

Figures 15 depicts a simple summary of Figures 13 and 14 at only the erosion condemnation governing the 1.6-meter from RFT peak eroded position. Cumulative erosion versus cumulative equivalent M829E3 rounds at 1.6-meters from RFT is plotted. For the respective 49°C, 21°C, -32°C, and equal distribution cases at this position, achievement of the

0.13-mm gun steel gas wash onset depth is at about 75, 120, 110, and 95 rounds, while achievement of the 5-mm erosion condemnation depth is at about 240, 390, 350, and 315 rounds.

The main focus of this report is for cannons with a mixture of experimental ablative M829E3 rounds and other kinetic energy-type rounds. When HEAT rounds are added to this mixture, their noticeable fin gouging of the chromed bore surface for the first 0.3-meter of bore travel past the forcing cone produces additional/higher frequency HC chromium cracking/pitting. This additional/higher frequency HC chromium cracking/pitting is not present when HEAT-type rounds are absent. The maximum gouging is centered at the 0.6-meter from RFT position, and diminishes after 0.3-meter of travel down bore. For experimental M829E3 rounds, since increased crack/pit frequency linearly increases the rate of erosion, the presence of HEAT round gouging allows erosion to peak at the 0.6-meter from RFT position instead of the normal 1.6-meter from RFT peak eroded position when these HEAT-type rounds are absent.

Cannon erosion often does not correlate with maximum crack depth, since ablatives and combustible cases unevenly alter erosion patterns and this erosion may unevenly alter (blunt) crack tips as a function of axial position. Cannon erosion often does not correlate with maximum transformation depth, again since ablatives and combustible cases unevenly alter erosion patterns, the heat is used unevenly at the surface and interface, and not all this heat gets into the steel substrate as a function of axial position. Cannon erosion always correlates with maximum interface degradation and substrate exposure. These generalizations hold for tank, artillery, and medium caliber gun cannons, and our coatings erosion model adjusts for any variations.

REFERENCES

1.   Dunn, S., Sopok, S., Coats, D., O'Hara, P., Nickerson, G., and Pflegl, G., "Unified Computer Model for Predicting Thermochemical Erosion in Gun Barrels," *Proceedings of 31st AIAA Joint Propulsion Conference*, San Diego, CA, July 1995; Also *AIAA Journal of Propulsion and Power*, Volume 15, Number 4, pp. 601-612.

2.   Sopok, S., "Cannon Coating Erosion Model with Updated M829E3 Example," *Proceedings of 36th AIAA Joint Propulsion Conference*, Huntsville, AL, July 2000.

3   Sopok, S., Loomis, R., Pflegl, G., and Rickard, C., "Preliminary Erosion Analysis for the Experimental M829E3 Kinetic Energy Round," *Proceedings of the 36th JANNAF Combustion Meeting*, NASA Kennedy Space Center, FL, October 1999.

4.   Coats, D., Dunn, S., and Sopok, S., "A New Chemical Equilibrium Code with Compressibility Effects," *Proceedings of the 33rd JANNAF Combustion Meeting*, Monterey, CA, October 1996.

5.   Gough, P., "The XNOVAKTC Code," Paul Gough Associates, Portsmouth, NH, U.S. Army BRL-CR-627, February 1990.

6.   Levine, J., "Transpiration and Film Cooling Boundary Layer Computer Program (MABL) - Numerical Solution of the Turbulent Boundary Layer Equations with Equilibrium Chemistry," NASA Marshall N72-19312, June 1971.

7.   Dunn, S., "Materials Ablation Conduction Erosion Program (MACE)," Software and Engineering Associates, Inc., Carson City, NV, June 1989.
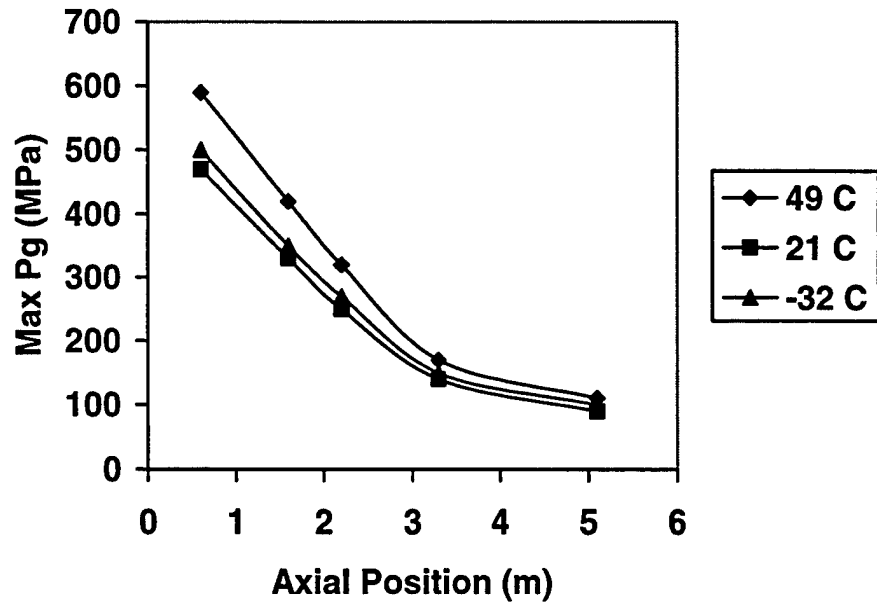
Figure 1. M829E3 NOVA gas pressure.
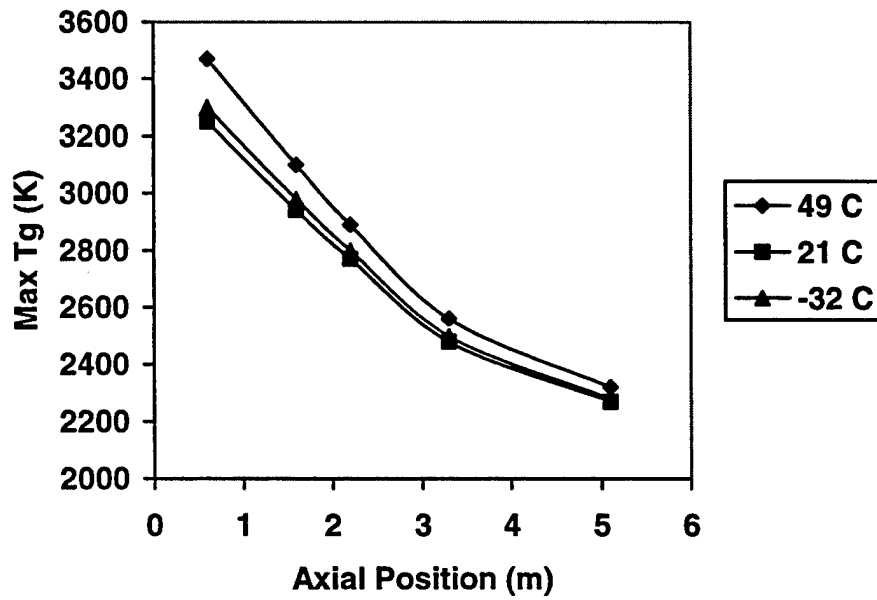
Figure 2. M829E3 NOVA gas temperature.
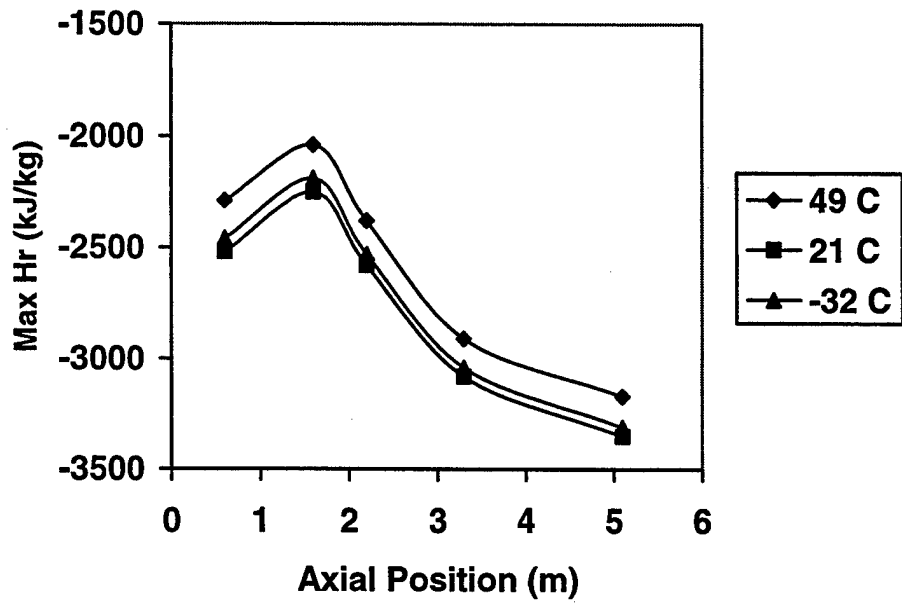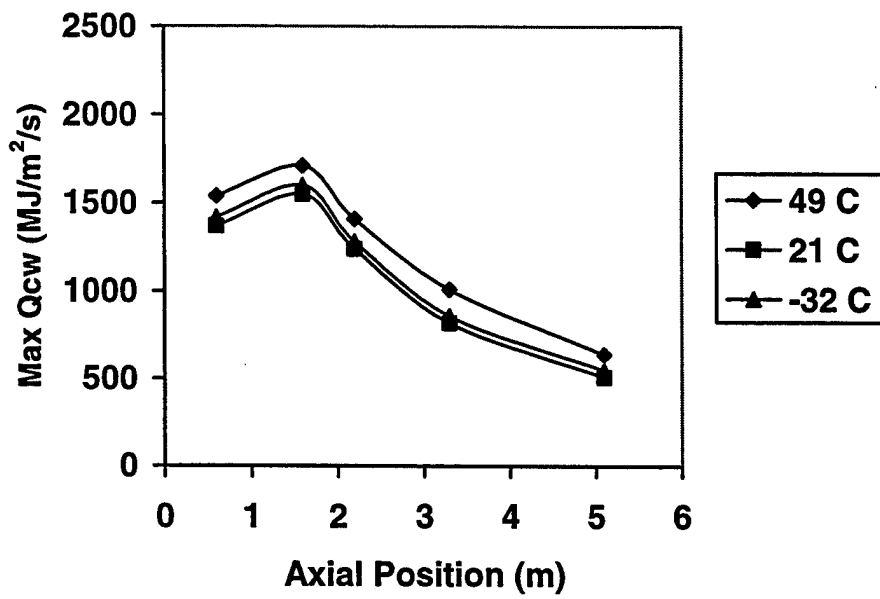
Figure 3. M829E3 MABL recovery enthalpy.

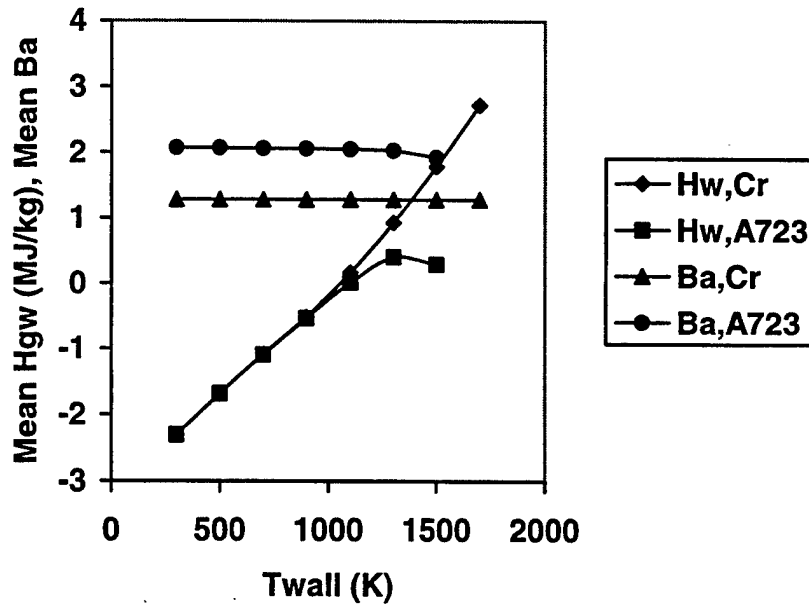Figure 4. M829E3 MABL cold wall heat flux.

13

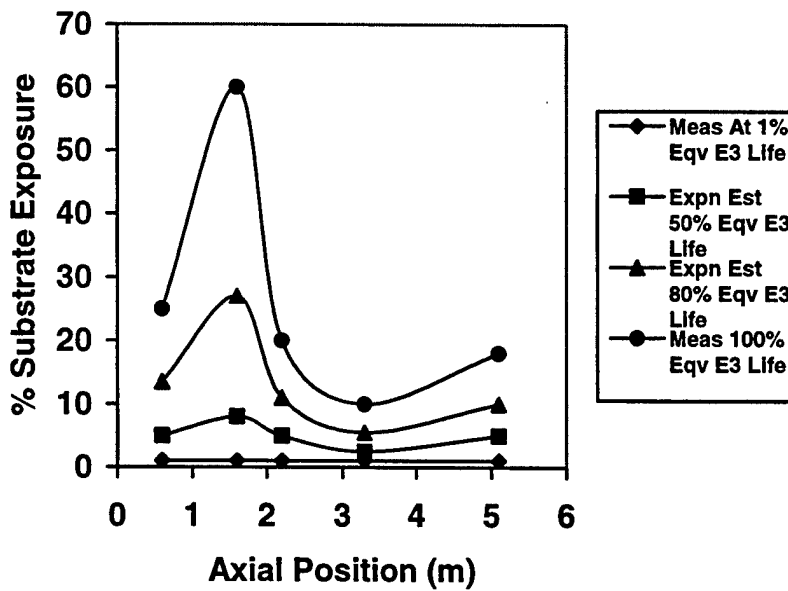Figure 5. M829E3 CCET gas/wall thermochemistry.

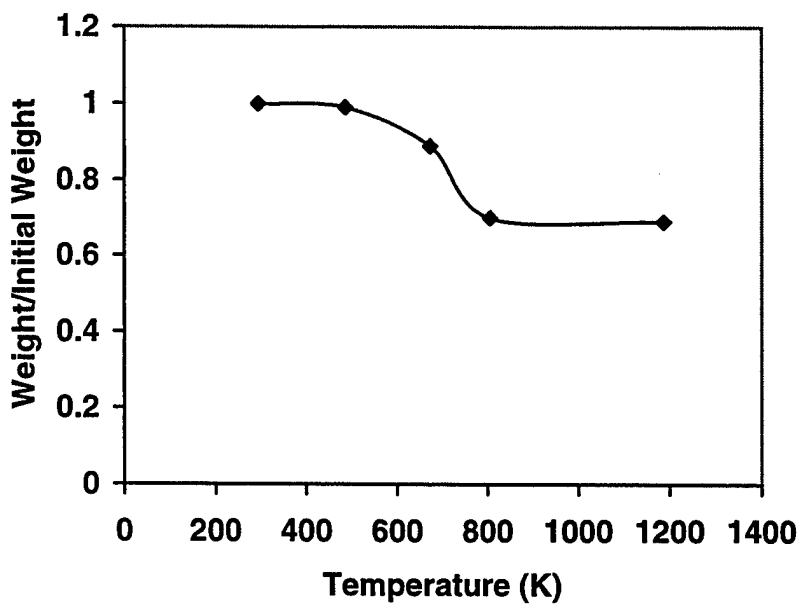Figure 6. M829E3 M256 substrate exposure.
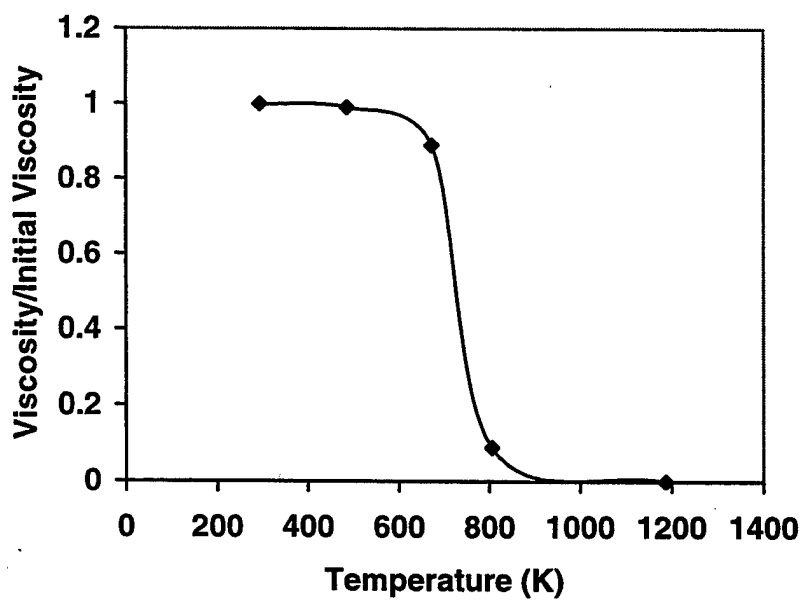
14

Figure 7. M829E3 ablative paste decomposition.

Figure 8. M829E3 ablative paste viscosity.

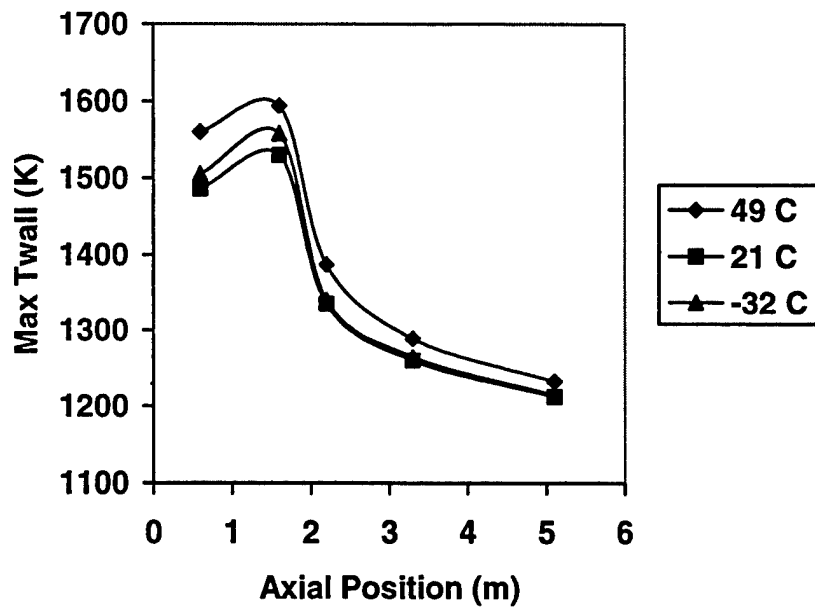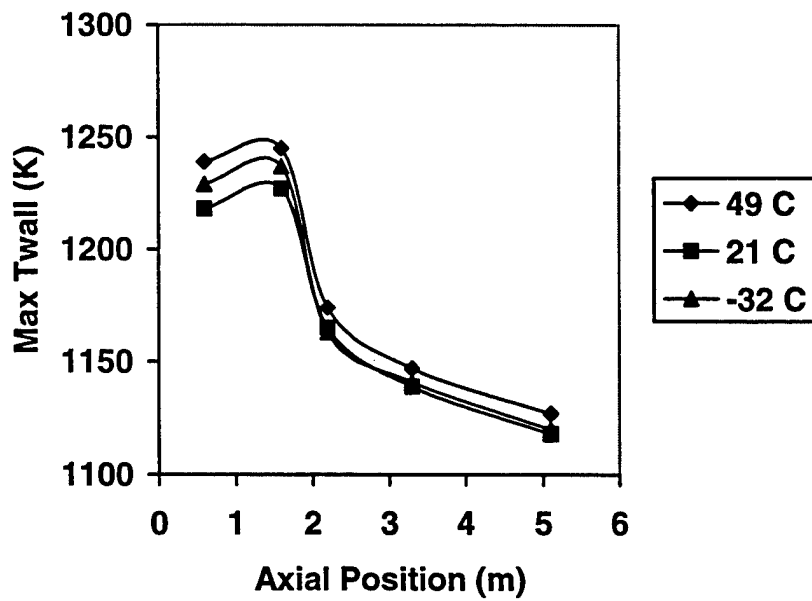Figure 9. M829E3 MACE HC chromium surface temperature.

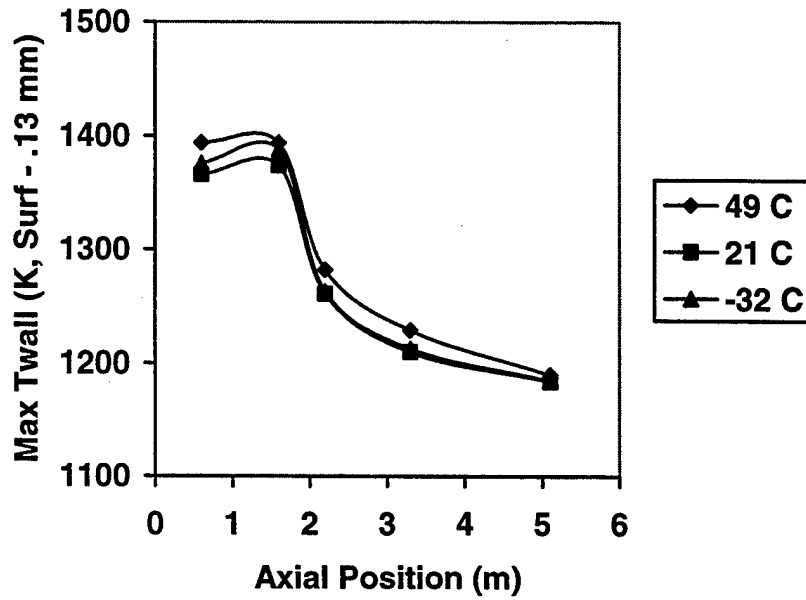Figure 10. M829E3 MACE A723 interface temperature.

Figure 11. M829E3 MACE A723 surface temperature.
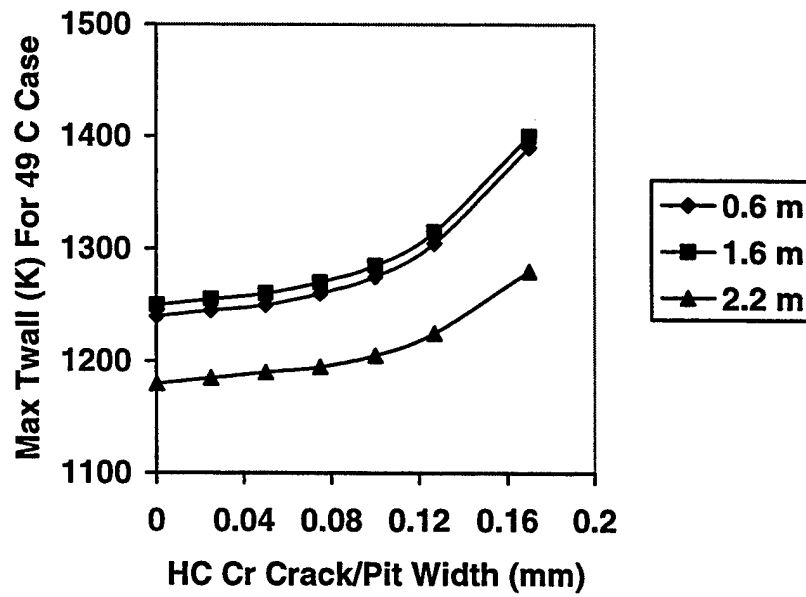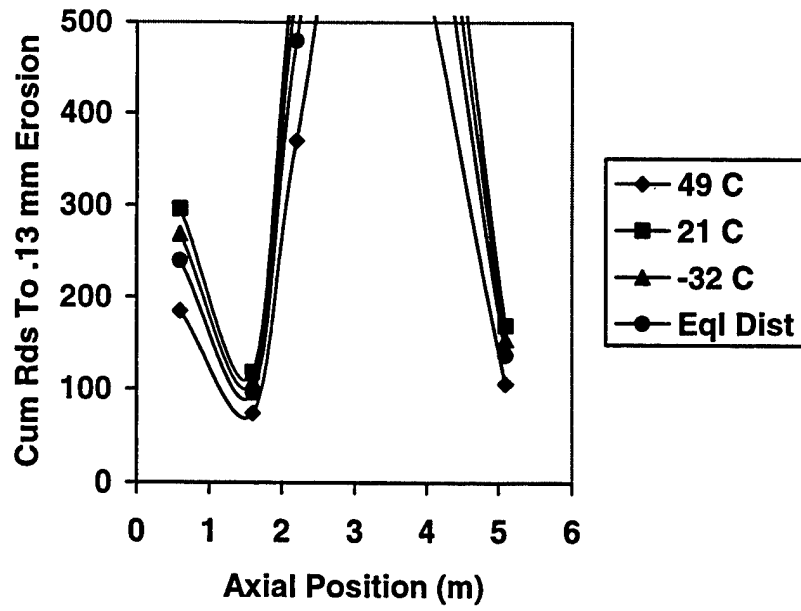

Figure 12. M829E3 exposed interface temperature.

Figure 13. M829E3 erosion onset.

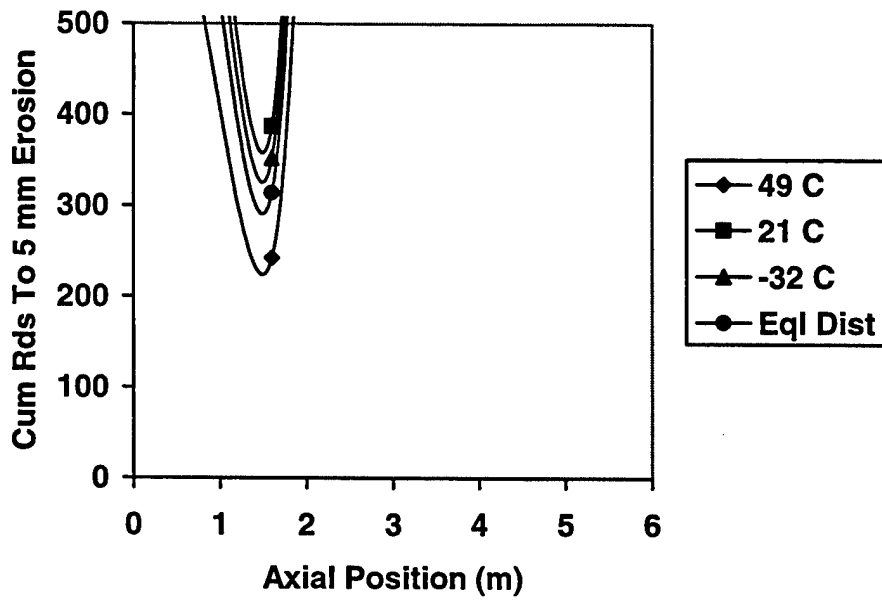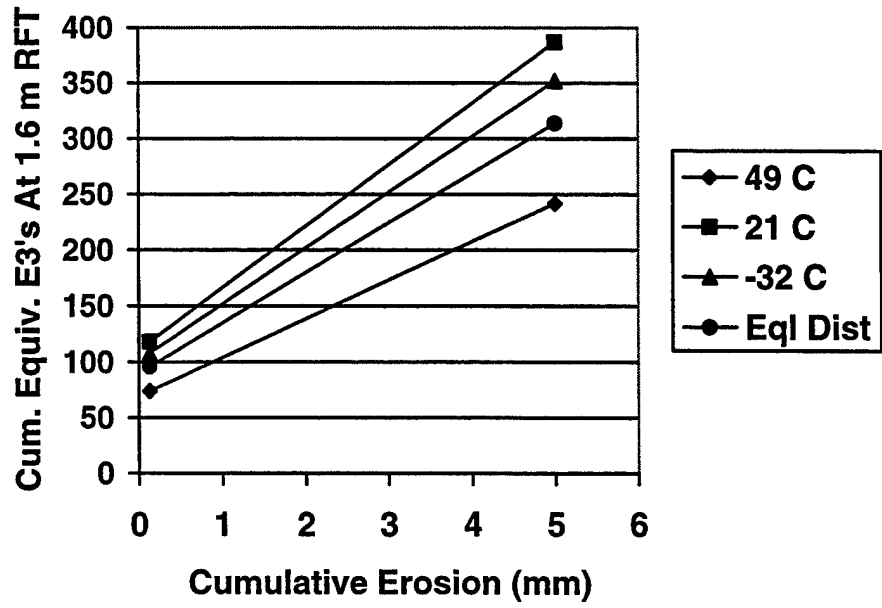Figure 14. M829E3 erosion condemnation.

Figure 15. M829E3 erosion summary.

TECHNICAL REPORT INTERNAL DISTRIBUTION LIST

	NO. OF COPIES
TECHNICAL LIBRARY ATTN: AMSTA-AR-CCB-O	5
TECHNICAL PUBLICATIONS & EDITING SECTION ATTN: AMSTA-AR-CCB-O	3
OPERATIONS DIRECTORATE ATTN: SIOWV-ODP-P	1
DIRECTOR, PROCUREMENT & CONTRACTING DIRECTORATE ATTN: SIOWV-PP	1
DIRECTOR, PRODUCT ASSURANCE & TEST DIRECTORATE ATTN: SIOWV-QA	1

NOTE: PLEASE NOTIFY DIRECTOR, BENÉT LABORATORIES, ATTN: AMSTA-AR-CCB-O OF ADDRESS CHANGES.

TECHNICAL REPORT EXTERNAL DISTRIBUTION LIST

<table>
<tr><td></td><td>NO. OF
COPIES</td><td></td><td>NO. OF
COPIES</td></tr>
<tr><td>DEFENSE TECHNICAL INFO CENTER
ATTN: DTIC-OCA (ACQUISITIONS)
8725 JOHN J. KINGMAN ROAD
STE 0944
FT. BELVOIR, VA 22060-6218</td><td>2</td><td>COMMANDER
ROCK ISLAND ARSENAL
ATTN: SIORI-SEM-L
ROCK ISLAND, IL 61299-5001</td><td>1</td></tr>
<tr><td>COMMANDER
U.S. ARMY ARDEC
ATTN: AMSTA-AR-WEE, BLDG. 3022
    AMSTA-AR-AET-O, BLDG. 183
    AMSTA-AR-FSA, BLDG. 61
    AMSTA-AR-FSX
    AMSTA-AR-FSA-M, BLDG. 61 SO
    AMSTA-AR-WEL-TL, BLDG. 59
PICATINNY ARSENAL, NJ 07806-5000</td><td>1
1
1
1
1
2</td><td>COMMANDER
U.S. ARMY TANK-AUTMV R&D COMMAND
ATTN: AMSTA-DDL (TECH LIBRARY)
WARREN, MI 48397-5000</td><td>1</td></tr>
<tr><td>DIRECTOR
U.S. ARMY RESEARCH LABORATORY
ATTN: AMSRL-DD-T, BLDG. 305
ABERDEEN PROVING GROUND, MD
  21005-5066</td><td>1</td><td>COMMANDER
U.S. MILITARY ACADEMY
ATTN: DEPT OF CIVIL & MECH ENGR
WEST POINT, NY 10966-1792</td><td>1</td></tr>
<tr><td>DIRECTOR
U.S. ARMY RESEARCH LABORATORY
ATTN: AMSRL-WM-MB (DR. B. BURNS)
ABERDEEN PROVING GROUND, MD
  21005-5066</td><td>1</td><td>U.S. ARMY AVIATION AND MISSILE COM
REDSTONE SCIENTIFIC INFO CENTER
ATTN: AMSAM-RD-OB-R (DOCUMENTS)
REDSTONE ARSENAL, AL 35898-5000</td><td>2</td></tr>
<tr><td>COMMANDER
U.S. ARMY RESEARCH OFFICE
ATTN: TECHNICAL LIBRARIAN
P.O. BOX 12211
4300 S. MIAMI BOULEVARD
RESEARCH TRIANGLE PARK, NC 27709-2211</td><td>1</td><td>COMMANDER
U.S. ARMY FOREIGN SCI & TECH CENTER
ATTN: DRXST-SD
220 7TH STREET, N.E.
CHARLOTTESVILLE, VA 22901</td><td>1</td></tr>
</table>

NOTE: PLEASE NOTIFY COMMANDER, ARMAMENT RESEARCH, DEVELOPMENT, AND ENGINEERING CENTER, BENÉT LABORATORIES, CCAC, U.S. ARMY TANK-AUTOMOTIVE AND ARMAMENTS COMMAND, AMSTA-AR-CCB-O, WATERVLIET, NY 12189-4050 OF ADDRESS CHANGES.